DOI: https://doi.org/10.37434/tpwj2024.05.03

CONSUMABLE AND NONCONSUMABLE ELECTRODE WELDING OF HIGH-STRENGTH 2219-T31 ALUMINIUM ALLOY

T.M. Labur, A.G. Pokliatskyi, V.A. Koval

E.O. Paton Electric Welding Institute of the NASU
11 Kazymyr Malevych Str., 03150, Kyiv, Ukraine

ABSTRACT

The influence of the conditions of nonconsumable (TIG) and consumable (MIG) electrode arc welding of high-strength aluminium alloy of 2219-T31 grade (USA) 5 mm thick was studied. Effective welding modes were selected by the main characteristics: absence of coarse defects, weld form factor, standard mechanical properties, and features of fracture surface relief. The strength level of welded joints after welding is 25–30 % lower compared to base metal (σ_t = 366–370 MPa). The impact toughness values of the welds after TIG welding vary from 16.4 to 20.3 J/cm^2, according to the rolling direction. Bend angle is almost 3 times lower than the base metal value (180 and 177°). Fracture of joints with technological reinforcement and of the weld root occurs along the boundary of weld fusion with the base metal, and at a distance from the surface — along the weld axis. The relief retains a predominantly cellular structure. Analysis results were used to establish the technological conditions of achieving an optimal quality of welds and the type of shielding gas for welding.

KEYWORDS: aluminium alloy, nonconsumable and consumable electrode welding modes, inert gases: argon, helium, welded joints, mechanical properties, investigations

INTRODUCTION

The main requirement in ensuring the reliability and performance of the structure is the weld quality. Analysis of standard welding technologies, widely used in fabrication of lightweight structures, shows that, in addition to selection of the welding process, its cost, the degree of processing and mastering in production the normative documents, required to reproduce the technologies under shop conditions, is also taken into account. Here, greater attention is paid to technological convenience of the process in the shop. However, the arc phenomena, deposition rate, as well as the possibility of precise control of the process remain to be the decisive factors for improvement of the efficiency of application of the selected arc welding technology. Certainly, saving on structural materials cost and energy consumption, as well as the possibility of process robotization are taken into account. The above requirements are now considered as key ones to increase the efficiency of welded structure fabrication, ensuring the conditions for reproducible quality of welds, saving the expenses and possibility of working without human intervention [1–3].

Nonconsumable (TIG) and consumable (MIG) electrode welding in different shielding gases (argon and helium), plasma-arc and hybrid joining processes are the most in demand for fabrication of lightweight structures from aluminium alloys [4–6]. The first technology is realized at a low speed, which is due to the mechanism of wire feed into the metal pool. With this method, a good formation of the welds is observed, as the arc is burning in a stable manner even at a low electric current density [4, 5]. Pulsed modes ensure intensive refinement of oxide inclusions at simultaneous degassing of the welds, and promote their wide acceptance in structure fabrication [2]. Plasma-arc welding method allows producing a sound joint of thin sheets, but this process remains to be costly, and it does not demonstrate any flexibility in manufacture [1]. Low heat input at MIG improves the efficiency of welding parts and components from aluminium alloys, and the process lends itself easily to automation and integration into the production line [1]. The main disadvantage of this technology remains to be a process of electrode metal heating insufficiently stable in time and space, as the arc length and position of its spot on the surface change alternately. It influences the mechanism of formation of molten metal drop, its size and nature of transition into the weld pool to fill the gap between the parts [3]. In addition, it influences the type of shielding atmosphere — argon or helium (Figure 1). Gas replacement increases the ability of the arc to penetrate the metal, input energy value, and the number of electrode drops decrease 1.5–2 times, average pool temperature, duration of its existence and degree of its degassing are increased. On the other hand, evaporation of volatile elements is decreased, and no pores form at the liquid drop stage [4].

Aluminium alloy of 2219 grade of Al–Cu–Mn (6.8 % Cu–0.32 % Mn–0.16 % Zr) alloying system belongs to the class of heat-hardenable and has a high

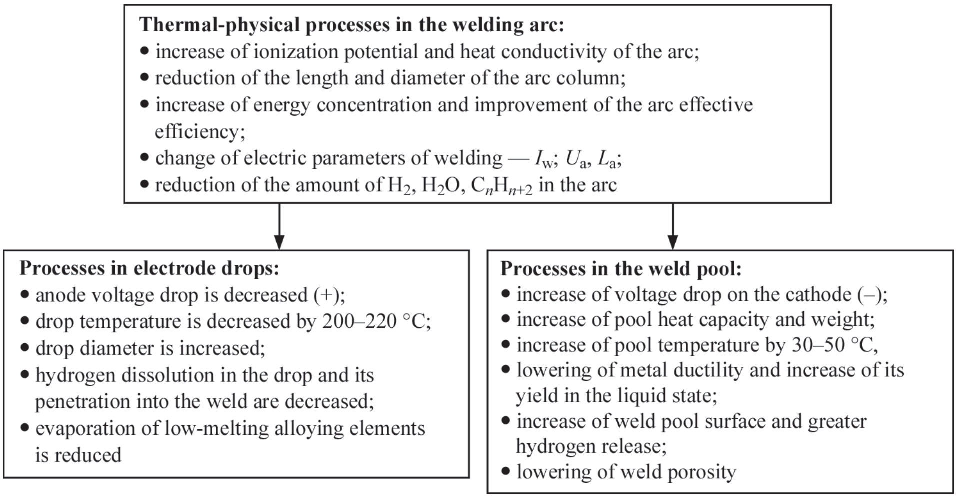

Figure 1. Thermal-physical processes arising in the arc, electrode metal drops, and in the weld pool at argon replacement by helium

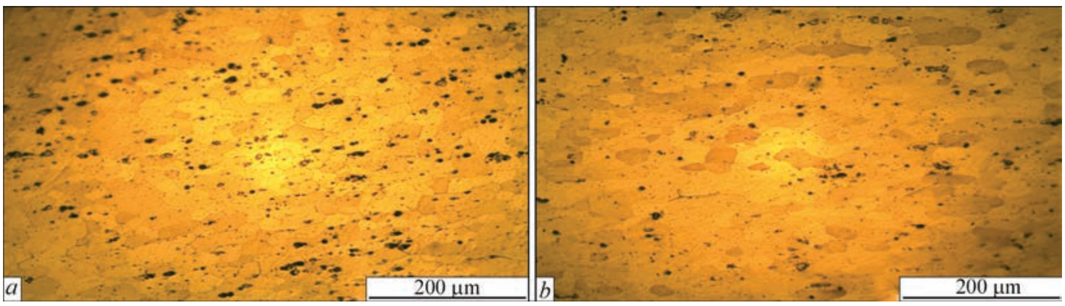

Figure 2. Microstructure of 2219-T31 alloy 5 mm thick along (*a*) and across (*b*) the rolling direction

specific heat [3]. High technological plasticity in the cold and hot state and adequate cold resistance distinguish it among the other alloys [4]. Under the conditions of superlow temperatures, including the temperature of –269 °C, the alloy strength and ductility become higher, making 2219 alloy unique for products, exposed to a broad temperature range in service [1]. A good combination of technological and physical-mechanical properties (Table 1) makes it highly popular in aerospace industry, as well as in structures of cylinders and tanks for liquid gas storage.

The above-mentioned technological and service properties are achieved due to the main alloying elements of 221-T31 alloy, namely copper and manganese. The alloy microstructure consists of aluminium-rich α-phase (solid solution) and stable θ($CuAl_2$)-phase (Figure 2). Intermediate phases include θ-′($CuAl_2$) and S′(Al_2CuMg), and presence of θ(Al_2Cu), T($Al_{12}Mn_2Cu$), Al_3Zr and $Al_{11}V$ phases provides the respective level of physical-mechanical properties both of the alloy proper, and of its welded joints. Semi-finished products are supplied to the manufacturer in the annealed (0), hardened and naturally aged (T3) or quenched and artificially aged state (T8), which is determined by tactical-technical and cost parameters of the respective welded structures and their operation conditions.

At the same time, under the conditions of technological heating, including the welding processes, 2219 alloy (similar to its Russian analog 1201), demonstrates sensitivity to the temperature level, which is due to the mechanism of solid solution decomposition and morphology of phase precipitation location, and ratio of their volume fraction in the structure [2–4]. Segregation of alloying elements and admixtures along the boundaries of weld crystallites and base metal grains results in formation of a heterogeneous structure, lowering the joint strength by 30–40 %. Welding speed affects the morphology of weld microstructure, as the temperature gradient on the interface of solid solution of liquid metal and phases, as well as the nature of distribution of alloying elements through the weld volume depend on it [3]. At metal overheating formations of brittle interlayers from oversaturat-

Table 1. Mechanical properties of 5 mm sheets of 2219-T31 aluminium alloy

Orientation	$\sigma_t^{b.m}$, MPa	$\sigma_{0.2}^{b.m}$, MPa	δ, %	α, deg	a_n, J/cm^2
Along the rolling direction	368	259.4	24.4	180	30.0
Across the rolling direction	369.6	270.4	22.0	177	23.1

ed phases develop between the grains, particularly on the fusion boundary with the base metal, where they sometimes form a dense frame around the grains. To reduce the heat input, it is recommended to apply concentrated heat sources and, as far as possible, increased welding speeds that ensures minimal level of heat input into the metal, its accelerated cooling, and less strength loss [6–8].

The objective of this work is determination of optimal conditions of welding the rocket load-carrying element set from aluminium alloy of 2219-T31 grade by TIG and MIG methods.

EXPERIMENTAL PROCEDURE

Before welding, the sheet blanks from 2219-T31 alloy were degreased with further chemical etching in a sodium hydroxide solution with multiple rinsing in hot and cold water. Blank lightening was performed in a nitric acid solution with further washing in running water. The blanks were dried naturally, which was followed by scraping the end faces and surfaces of the edges to be welded (approximately 15 mm wide) to the depth of 0.1 mm with the purpose of prevention of oxide film inclusions and gas pores in the welds.

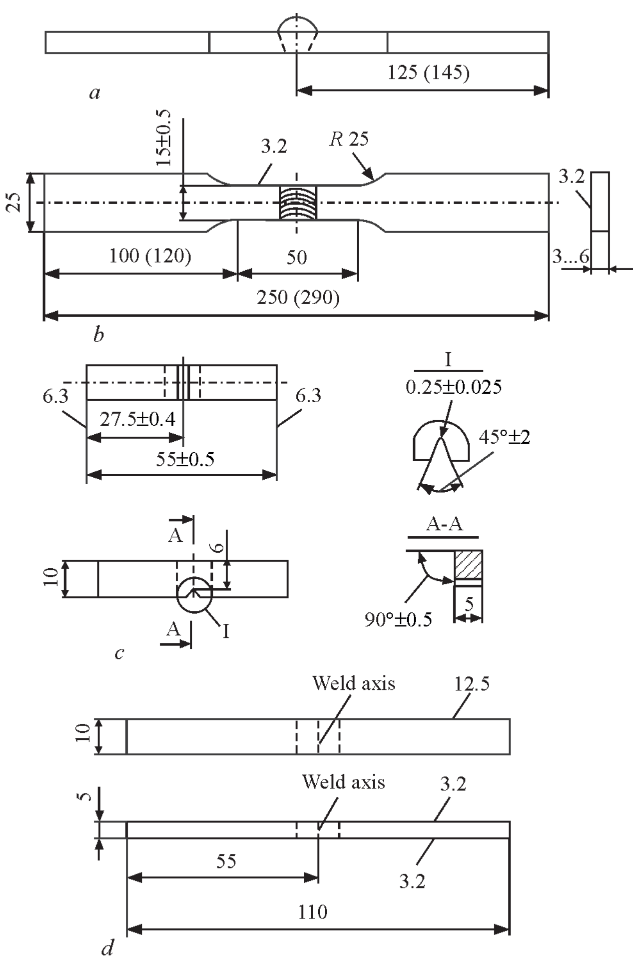

Figure 3. Drawings of samples which were used to determine the mechanical properties of welded joints: *a* — ultimate strength of welded joint ($\sigma_t^{w.j}$); *b* — ultimate strength of weld metal ($\sigma_t^{w.m}$); *c* — impact toughness of weld metal; *d* — welded joint bend angle

The quality of weld formation was controlled by their appearance. Internal quality of the welds was assessed by the results of detection of defects of the type of cracks, lacks-of-penetration, and pores by roentgenography (GOST 7512–89). X-ray unit RAP-150/300 was used for this purpose, and the density of weld metal was assessed in Densitometr instrument. Control results allowed selection of optimal modes of the welding process, when no coarse defects form.

After welding 2219-T31 alloy the produced butt joints were examined, and measurement of the main geometrical parameters of the welds was conducted. Geometrical parameters of the welds (B is the weld width from the joint face surface, H is the weld width from the joint reverse surface (weld root), δ is the base metal penetration depth (in this case it is equal to its thickness), b is the height of technological reinforcement convexities, h is the weld root height) was determined using electronic caliper ART-34460-150, which had the division price of 0.01 mm, and measurement accuracy of 0.03 mm.

Qualitative assessment of the change in the values of strength, ductility and toughness of welded joints of 2219-T31 alloy, depending on the studied arc welding processes, was performed by the results of mechanical testing of standard samples (GOST 1497–84) using all-purpose TsD-4 machine with 2T scale. Testing was conducted on samples of XIII type to GOST 6996–66. Sample drawings with dimensions are given in Figure 3. Tensile testing and determination of strength values of the joints ($\sigma_t^{w.j}$) were conducted using flat samples with technological reinforcements on the face side with removed weld root. Evaluation of weld metal strength ($\sigma_t^{w.m}$) was preformed on samples without reinforcement or weld root, which were mechanically removed from the test sample surface. Mechanical tests of the above-mentioned samples were conducted under stationary conditions and their ultimate strength values were calculated ($\sigma_t^{w.j}$ and σ_t^{w}). Sample load was here uniformly distributed over the entire working part, in keeping with the requirements of GOST 1497–73.

Strength value determined experimentally allowed calculation of strength coefficients of the joints and establishing the level of their sensitivity to the thermal cycle of welding under TIG and MIG conditions. The degree of their influence on the condition of metal in the welds with technological reinforcement and without it is characterized by the joint strength coefficient, calculated as $K_w = \sigma_t^{w.j}/\sigma_t^{b.m}$ or $K_w = \sigma_t^{w.m}/\sigma_t^{b.m}$.

General state of the metal and its deformability after the thermal cycle of welding was assessed using the technological testing method — bend angle (a). This ductility value was determined on samples of base metal and welded joints under the conditions of three-point bending with load application from the weld root side. Technological reinforcement and weld root were here removed by machining to the required dimensions (Figure 3).

Impact toughness value (a_n) allowed determination of brittle fracture susceptibility of the joint metal. Its experimental determination was performed using the respective scheme of loading samples with a sharp notch of radius $R = 0.25$ mm (Charpy) along the weld axis, in keeping with the requirements of GOST 9454–76. Average value of this characteristic was determined by the results of testing three samples.

Modern analysis procedures were used to substantiate the produced experimental results of comprehensive investigation of the mechanical properties of welded joints of 2219-T31 alloy. Their systematization and plotting of graphical dependencies were performed using modern computer technologies, including Smage Pro and Statistica 5.0 programs.

INVESTIGATION RESULTS AND THEIR DISCUSSION

In order to form an appropriate technological reinforcement of the welds, using 1.6 mm welding filler wire of 2319 grade it was found that higher quality joints can be produced by TIG method at 12 m/h speed of welding 2219-T31 alloy. The value of welding current here was equal to 290 A. Considering the risks of defect development in the welds (tungsten inclusions), especially when making extended welds, 6 mm tungsten electrode (GOST 23949) with lanthanum oxide or yttrium oxide was used for welding. The distance from the edge of the nonconsumable electrode to the surface of the edges being welded was equal to 4 mm.

Table 2. Tentative modes of automatic nonconsumable electrode welding of 2219-T31 aluminium alloy 5 mm thick

Tungsten electrode diameter, mm	Filler wire diameter, mm	Welding current value, A	Welding speed, m/h	Argon flow rate, l/min
6.0	1.6	290	12.0	15–17

Butt welds were made on blanks of 300×150×5 mm size, which were cut out of sheet semi-finished products along and across the rolling direction, without scraping the edges on the backing. Filler wire feed rate was equal to 128–130 m/h. Welding of the metal from one side was performed without edge preparation. The angle of the torch inclination relative to weld axis was equal to 10–15°, the distance between the torch nozzle and metal being welded was equal to 8–12 mm. Arc length (distance between the metal and wire tip) was equal to 3–5 mm.

Automatic argon-arc welding (TIG) was performed from MW-450 power source of Fronius Company, Austria, which ensures maximal value of welding current of 450 A and allows making extended welds at the required current level. Used for this purpose was symmetrical square wave alternating current of 200 Hz frequency, which will ensure a high degree of cathode cleaning of the edges being welded and stability of performance of 2219-T31 alloy joining process [3]. Tentative modes of welding 2219-T31 alloy 5 mm thick are given in Table 2.

Complete penetration of the edges being welded without their scraping was achieved in one pass. Formation of the back bead, i.e. weld root, occurred at application of a replaceable stainless steel backing with an elliptical shape of the groove of 1 mm depth and 6 mm width. Reliable shielding of the welding zone was ensured by high purity argon (GOST 10157), the flow rate of which was equal to 15–17 l/min. TIG

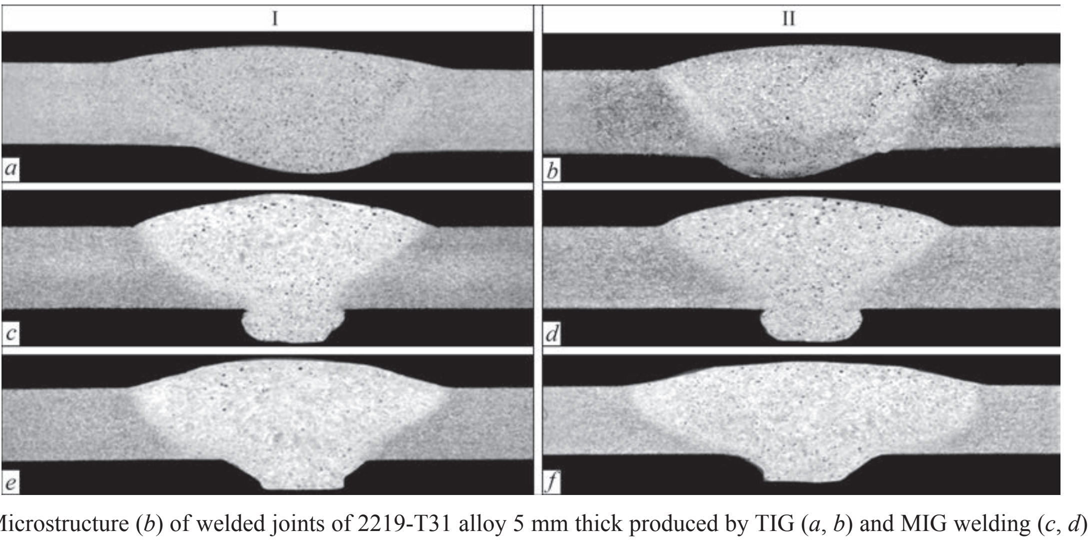

Figure 4. Microstructure (b) of welded joints of 2219-T31 alloy 5 mm thick produced by TIG (a, b) and MIG welding (c, d) in argon (c, d) and helium (e, f) along (I) and across (II) the rolling direction

welding technology was realized in the horizontal position by complete melting of base material and filler wire edges at heating by tungsten electrode arc. All the welding parameters were thoroughly controlled and measured to determine the optimal welding mode of 2219-T31 alloy 5 mm thick. The established mode allowed producing a smooth weld surface with gradual transition to the base metal (Figure 4).

Analysis of the appearance of butt joints and assessment of weld quality by X-ray method did not reveal any coarse defects of the type of cracks, lacks-of-penetration or porosity in the welds, produced by TIG (Figure 5, *a*). This is indicative of realization of appropriate thermal-physical conditions in welding, namely liquid metal solidification and sound weld formation. Application of different polarity

Shielding atmosphere	Rolling orientation	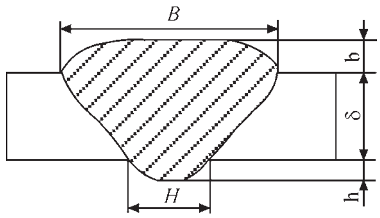				Weld form factor $K = \frac{B}{b+\delta}$	Sample appearance
		B	*b*	*H*	*h*		
TIG welding							
Argon	Along	16.04–16.55	0.91–0.95	8.56–9.03	1.27–1.32	2.75	
	Across	15.35–16.43	0.96–1.3	8.22–8.9	1.38–1.56	2.19	
MIG welding							
Argon	Along	13.3–14.15	1.61–1.70	5.45–5.72	1.85–1.92	2.09	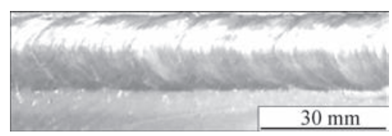
	Across	14.5–16.41	1.51–1.60	5.49–5.75	1.86–2.06	2.22	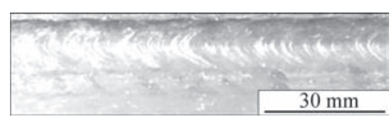
Helium	Along	13.9–15.10	1.44–1.67	6.38–7.21	1.84–1.95	2.21	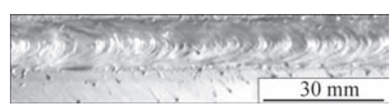
	Across	16.6–17.18	0.67–0.73	6.08–6.28	1.75–1.89	2.90	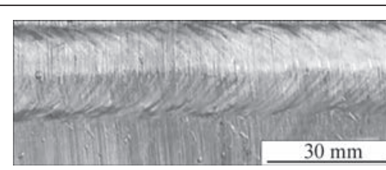

Notes. 1. Weld form factor (K) — ratio of weld width (B, mm) to its thickness ($b + \delta$), where B is the weld width, b is the reinforcement height, δ is the molten base metal depth; H is the weld root width, h is the reinforcement height from the weld root side, 2. K value is allowed in the range from 0.5 to 4. Values from 1.2 to 2 are regarded as optimal.

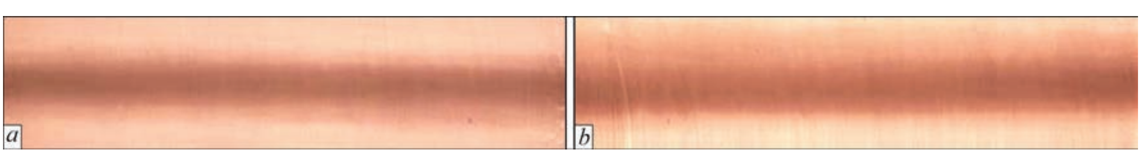

Figure 5. X-ray diffraction patterns of 2219-T31 alloy welds produced by TIG welding in argon along (*a*) and across the rolling direction (*b*)

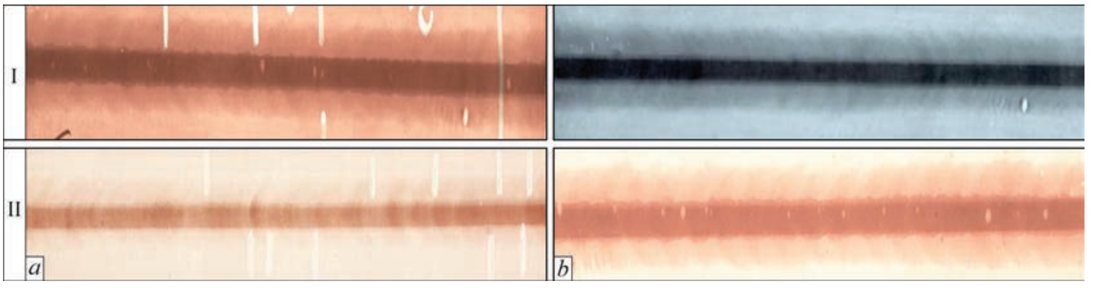

Figure 6. X-ray diffraction patterns of 2219-T31 alloy produced by MIG welding in argon (I) and helium (II) along (*a*) and across (*b*) the rolling direction

square wave current in modes, when reverse polarity prevails, ensures efficient degassing of the welds with such a welding process.

Modes of test alloy welding by MIG technology (Figure 3) were also optimized. Their essence is heating of 1.6 mm electrode (filler) wire of 2319 grade by the arc up to melting of its tip and filling of the gap between the edges of blanks being welded by liquid metal. Presence of a replaceable backing from stainless steel with a groove of elliptical shape of 1 mm depth and 6 mm width allowed achieving complete penetration of the edges being welded and forming the weld root in one pass (Figure 4), depending on shielding gas grade — argon (GOST 10157) or helium (GOST 20461, DSTU 141175:2004). Argon flow rate here was equal to 25 l/min, and of helium — 30 l/min.

Butt welds were produced in an argon or helium atmosphere by an arc from IUP-1 power source on blanks of 300×150×5 mm size, which were cut out of sheet semi-finished products along and across relative to the direction of rolling. Visual control of the quality of weld formation showed absence of coarse defects of the type of cracks and lacks-of-penetration in the test alloy butt joints produced by a consumable electrode, but defects in the form of pores were recorded after X-ray inspection. As evidenced by X-ray diffraction patterns of butt joints (Figure 6) produced by MIG in argon, pores of 1 to 2 mm diameter form in the zone of technological reinforcement at liquid metal crystallization, i.e. the welding conditions did not provide its proper degassing. Different factors can be the source of their formation, including temperature conditions of the environment, higher humidity of shielding gas, etc. Porosity can also be caused by segregation of elements present in the composition of 2219-T31 alloy, as a result of structural transformations of the liquid weld metal. In order to prevent porosity, it is necessary to thoroughly clean the base metal and filler wire from oxides or contamination.

Complete penetration of joints welded by MIG technology in argon, was produced in the mode, when the welding current value was 165–170 A, and arc voltage was 24–25 V. Welding speed was equal to 28–29 m/h. Higher density of welding current enhanced the metal penetrability by the arc. The extent of the arc immersion into the liquid metal of the weld pool is increased, and it has a positive impact on formation of welds of smaller dimensions. It occurred due to high specific arc power and temperature level in the metal region of the impact of an active heating spot, which allowed increasing the process speed, compared to TIG welding [1, 2].

At helium application as shielding atmosphere in MIG welding of 2219-T31 alloy formation of higher quality welds is observed. This is related to the fact that compared to argon, helium provides the thermal-physical conditions of stable realization of the arc process: it promotes increase of metal penetration depth. High concentration of thermal energy at helium-arc welding is ensured by reliable arc excitation and its stable burning, which determines the quality of "cathode" cleaning of the surfaces of the weld and of the zone near it. Owing to a high ionization potential and heat conductivity, the volumes of electrode metal sputtering are reduced. At helium application the electric current was 120–135 A, and voltage was 34–36 V. Welding speed here was 25–27 m/h (Table 3).

Measurement of the geometrical parameters of welds in joints produced by MIG welding in argon, showed that their width varies in the ranges of 13.3–14.15 mm and 14.45–16.11 mm, and in helium it changes in the range of 13.90–15.10 mm, respectively. The dimensions of the weld root (penetration) are 10–15 % larger than in TIG welded joints. In samples

Table 3. Tentative modes of automatic consumable electrode arc welding of 2219-T31 aluminium alloy 5 mm thick in shielding gas atmosphere

Shielding atmosphere	Electrode wire diameter, mm	Welding current, A	Welding speed, m/h	Arc voltage, V	Gas flow rate, l/min
Argon	1.6	165–170	28–29	24–25	25
Helium	1.6	120–135	25–27	34–36	20

Table 4. Mechanical properties of welded joints of 2219-T31 aluminium alloy 5 mm thick made by argon-arc welding by TIG and MIG methods

Welding process	Shielding atmosphere	Weld orientation relative to rolling direction	$\sigma_t^{w.j*}$, MPa	$\sigma_t^{w.m**}$, MPa	α, deg	a_n, J/cm²	Strength factor K	
							$\frac{\sigma_t^{w.j}}{\sigma_t^{b.m}}$	$\frac{\sigma_t^{w.m}}{\sigma_t^{b.m}}$
Nonconsumable electrode	Argon	Along	255.2	241.9	60	16.3	0.69	0.66
		Across	258.0	240.9	58	19.4	0.70	0.65
Consumable electrode	Argon	Along	258.6	231.7	45	16.2	0.70	0.63
		Across	261.5	234.8 д	45	17.0	0.71	0.64
	Helium	Along	238.2	252.0	52	18.5	0.64	0.68
		Across	243.0	239.1	54	18.0	0.66	0.65

Notes. 1. Samples failed in the zone of weld fusion with base metal: 2. Sample fracture occurred in the weld metal. 3. Strength coefficient is given relative to base metal strength in the initial condition (2219-T31). $K = \frac{\sigma_t^{w.j}}{\sigma_t^{b.m}}$ — welded joint; $K = \frac{\sigma_t^{w.m}}{\sigma_t^{b.m}}$ — weld metal.

with technological reinforcement, a reverse dependence of its height on the shielding gas is observed. These values are 30–45 % higher in joints produced by MIG welding in argon. Weld root height, both in the first and second variants of shielding atmosphere differs 1.5 times. Weld form factor, in keeping with formula $K = B(b + \delta)$ for joints TIG welded along and across the rolling direction, is equal to 2.75 and 2.19, respectively, and for MIG welded joints it is 2.1 and 2.2 in argon, and 2.2 and 2.9 in helium. Comparing the results of measurement of geometrical dimensions of welds in TIG joints, cut out along and across the rolling direction, and in MIG joints made in argon or helium one can see that their values differ by 2–3 mm, respectively. Weld root dimensions are 10–15 % larger in TIG welded joints than in the joints produced under MIG conditions.

To assess the mechanical properties of the joints, produced by TIG using 1.6 mm 2319 welding wire, standard samples from defect-free weld regions were prepared, based on X-ray inspection results. Analysis of the results of their experimental testing showed (Table 4) that irrespective of the rolling direction, TIG joints with weld reinforcement fail along the zone of weld fusion with the base metal at static tension ($\sigma_t^{w.j}$) (Figure 7). Samples without technological reinforcement fail along the weld metal. Figure 8 shows fractures of samples of 2219-T31 welded joints produced by TIG in both the directions relative to rolling orientation. All the fractures demonstrate a ductile nature of the relief. Pitted structure of the fracture surface is indicative of the mechanism of nucleation, growth and coalescence of microvoids as a result of breaking up of the bridges between the crystallites.

Figures 9 and 10 show the characteristic fractures and special features of fracture surface of 2219-T31 alloy welded joints produced in argon and helium by MIG technology. The pattern of the sample surface depends on its type and loading mode at testing. In samples without technological reinforcement, fracture runs along the weld axis. Their relief is more ductile compared to relief of samples with technological re-

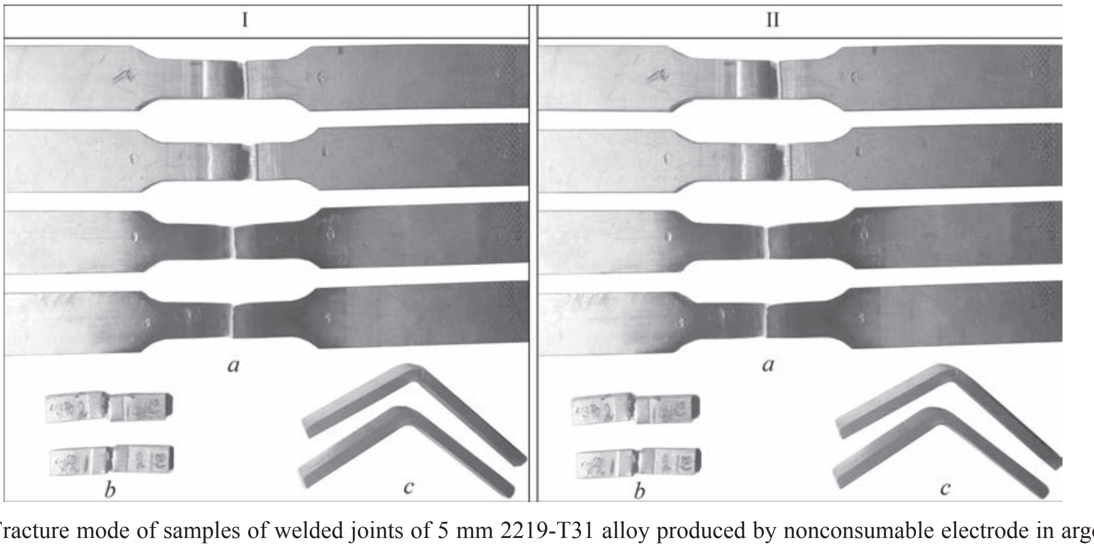

Figure 7. Fracture mode of samples of welded joints of 5 mm 2219-T31 alloy produced by nonconsumable electrode in argon along (I) and across (II) the rolling direction under the conditions of mechanical testing: *a* — uniaxial tension; *b* — impact toughness, *c* — three-point bending

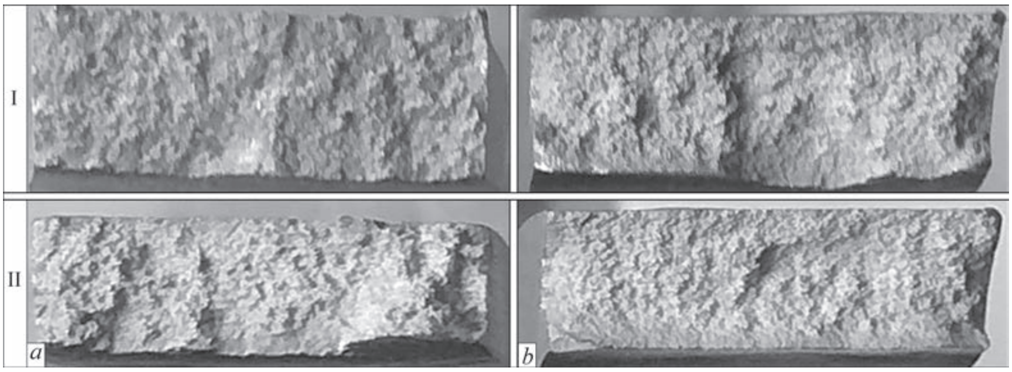

Figure 8. Fractures of samples of welded joints of 5 mm 2219-T31 alloy produced by nonconsumable electrode in argon along (I) and across (II) the rolling direction, after mechanical tensile testing: *a* — samples without reinforcement; *b* — samples with reinforcement

inforcement. They fail along the zone of weld fusion with base metal. Here, after TIG welding the ultimate strength of welded joints, where the weld was located along the rolling direction of the welded sheets, is on the level of 247–262 MPa, and in the weld located across the rolling direction it is in the range of 253–261 MPa, i.e. it decreased by almost 30 %, compared to the level of base metal strength.

Samples without technological reinforcement fail in the weld metal, where the ultimate strength ($\sigma_t^{w.m}$) at static tensile testing after welding is equal to 237–245 MPa under the conditions of the weld orientation along the rolling direction and 234–247 MPa at its location across the rolling direction. Impact toughness of the metal of welds produced in TIG welding along the rolling direction, varies from 15.9 to 16.9 J/cm^2, and across the rolling direction it changes from 17.5 to 22.4 J/cm^2, respectively. Bend angle of the mentioned welded joints is equal to approximately 60° (Table 4). In the case, when the samples have technological reinforcement, the ultimate strength of welded joints, produced by consumable electrode in helium at weld orientation along the rolling direction, is equal to 231–252 MPa, and at weld orientation across the rolling direction, it is at the level of 227–265 MPa. In welding in argon, the ultimate strength of welded joints is equal to 255–260 and 256–266 MPa at weld orientation along and across the rolling direction, respectively.

When helium is used in MIG welding, a similar dependence of the mode of fracture of test samples of welded joints is observed (Figure 10). The fracture surface has a predominantly ductile relief, which reflects the fine-dendritic structure of the welds. In samples with technological reinforcement, the relief on the fracture surface is more brittle, which is indicative of a higher degree of local deformation of the metal in the zone of weld fusion with the base metal. Welds made along the rolling direction, have the ultimate metal strength on the level of 254–259 MPa, and those welded across the rolling direction – on the level of 257–261 MPa. Bend angle values of joints welded in helium with weld location along the rolling direction decreased to 27–31°, and those across the

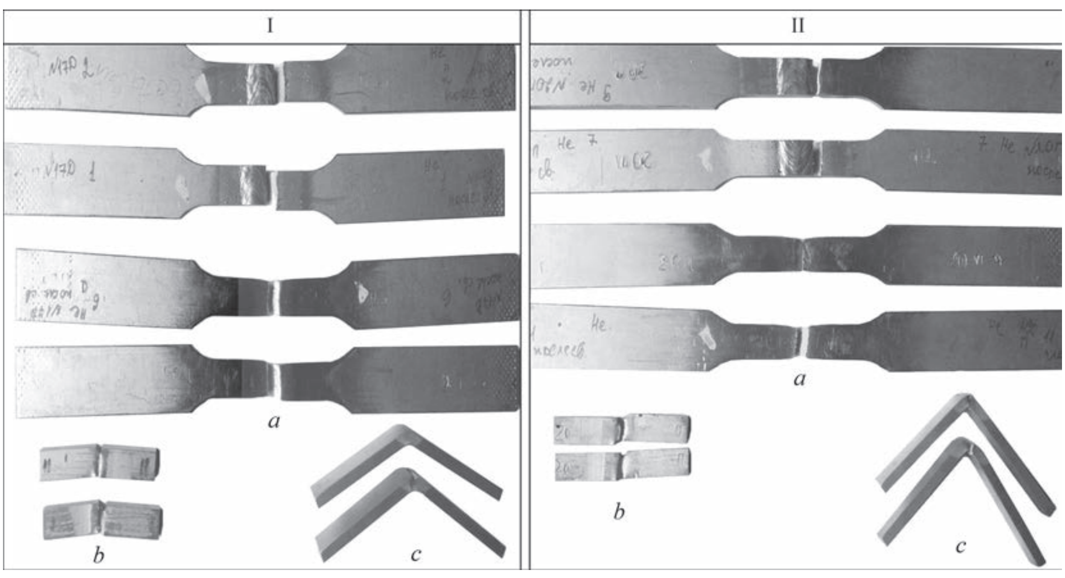

Figure 9. Fracture mode of samples of welded joints of 5 mm 2219-T31 alloy produced by consumable electrode in helium along (I) and across (II) the rolling direction, under the conditions of mechanical testing: *a* — uniaxial tension; *b* — impact toughness; *c* — three-point bending

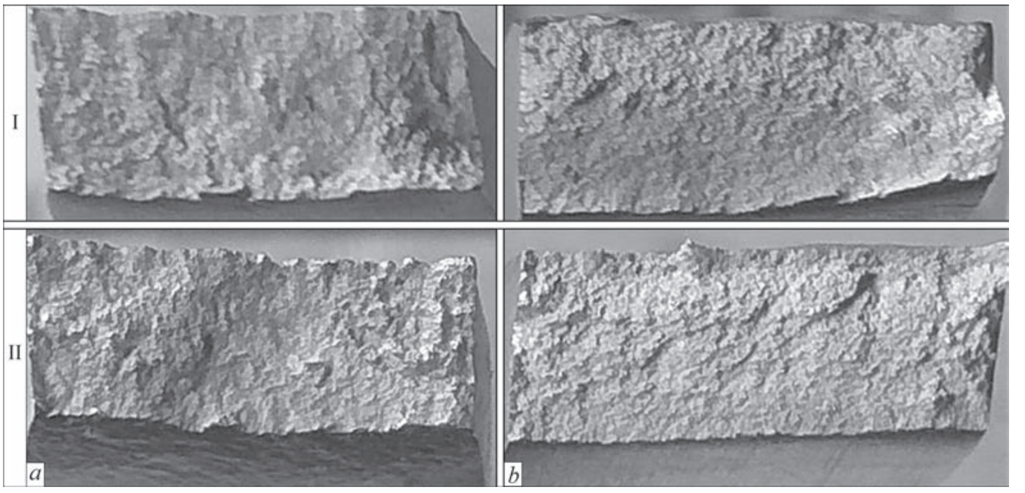

Figure 10. Fractures of samples of welded joints of 5 mm 2219-T31 alloy produced by consumable electrode in helium along (I) and across (II) the rolling direction, after mechanical tensile testing: *a* — samples without reinforcement; *b* — samples with reinforcement

rolling direction are 1.5 times higher (39–45°). The impact toughness value of the weld metal dropped to 12.9–13.5 and 12.3–12.9 J/cm^2, respectively.

Analysis of fracture surface morphology in welded joints produced both along and across the rolling direction, showed that their relief has a predominantly cellular structure. It forms as a result of microcrack initiation on coarse phase particles or intermetallic inclusions. The crack length is determined by the size of volume fraction in the base metal and depends on the TIG or MIG welding cycle. Optimal modes of welding 2219-T31 alloy promote formation of a homogeneous structure, which ensures the ductile mode of joint fracture under the test conditions.

CONCLUSIONS

1. Technological conditions of producing sound welds when joining 5 mm high-strength aluminium alloy of 2219-T31 grade at arc technologies of TIG and MIG welding were studied. It was found that optimal formation of sound welds without coarse defects is achieved under TIG conditions at electric current of 290 A and welding speed of 12 m/h. At MIG in argon atmosphere such welds can be produced using current I_w = 165–170 A and welding speed of 28 m/h, and in case of helium application — 120–135 A with the speed of 25–27 m/h, i.e. under the conditions, when power losses are 20–30 % lower. Weld form factor *b* in the joints, TIG welded along and across the rolling direction, is equal to 2.75 and 2.19, and in joints MIG welded in argon it is 2.1 and 2.2, and in helium — 2.2 and 2.9, respectively.

2. Level of alloy welded joint strength after TIG is equal to 255–258 MPa, that is 30 % lower compared to base metal (σ_t = 366–370 MPa). Under the conditions of MIG welding in argon joint strength value is equal to 258–261 MPa, and in helium it decreases (238–243 MPa). The above-mentioned occurs as a result of structural transformations of metal under the thermal-physical welding conditions, and it is also associated with appearance of eutectic interlayers and excess phases near the weld crystallite boundaries. The high probability of defect formation at argon application under MIG conditions, limits its application for critical parts and components.

3. Impact toughness value of TIG welds made along the rolling direction is equal to 15.9–16.9 and across the rolling direction it is 17.5–22.4 J/cm^2. Technological ductility (bend angle) of the joints is equal to 50 and 60°, respectively. After MIG welding in argon this value is almost the same, irrespective of the rolling direction (43–46 and 44–47°), in helium it is 50–55 and 53–57°, respectively, which is almost 3–4 times lower than the base metal value (180 and 177°). Impact toughness of welds after MIG welding in helium is 18.3–18.6 J/cm^2 along the rolling direction, and 17.5–18.4 across the rolling direction. In case of argon application a lowering of the value depending on the rolling direction is observed in the welds, 16.0–16.5 and 16.9–17.1 J/cm^2, respectively.

4. Fracture of joints of 2219-T31 alloy with technological reinforcement and weld root occurs along the boundary of the weld fusion with the base metal, and at a distance from the surface it runs along the weld axis. The relief retains a predominantly cellular structure, microcrack initiation, probably, occurs on the coarse phase particles or intermetallic inclusions, located along the boundaries of crystallites and metal grains, much more brittle than the aluminium matrix. The length of the primary crack depends on the volume fraction of the above-mentioned particles in the alloy and thermal-physical conditions of welding (TIG or MIG). It is found that formation of a more uniform structure of weld relief, when the proper joint strength and ductile mode of their fracture are pro-

duced, can be achieved with optimum modes for both the technologies.

REFERENCES

1. Beletsky, V.M., Krivov, G.A. (2005) *Aluminium alloys (Composition, properties, technology, application)*: Refer. Book. Ed. by I.N. Fridlyander. Kyiv, Komintekh [in Russian].
2. Albert, D. (1993) Aluminium alloys in arc welded constructions. *Welding World*, 32(**3**), 97–114.
3. Ishchenko, A.Ya., Labur, T.M. (2013) *Welding of modern aluminium alloy structures.* Kyiv, Naukova Dumka [in Russian].
4. Labur, T.M. (2022) Tendencies of technological development of arc welding processes for joining modern aluminium alloys. *Svarshchik,* **1**, 6–17 [in Russian].
5. Lobanov, L.M., Labur, T.M., Mazur, O.A. et al. (2022) Cost optimization of the methods of welding structures of fuel tanks for aerospace vehicles. *Avtomatych. Zvar*., **3**, 42–52 [in Ukrainian].
6. Nyrkova, L.I., Labur, T.M., Shevtsov, E.I. et al. (2022) Complex of properties of 2219 alloy weld joint in T62 state under modeling operating conditions. *Space Sci. & Technol.*, 28(**2**), 14–29.
7. Mashin, V.S., Poklyatsky, A.G., Fedorchuk, V.E. (2005) Mechanical properties of aluminium alloys in consumable and nonconsumable electrode arc welding. *The Paton Welding J.,* **9**, 39–45.
8. Kiyoto, S. (1993) Materials and joining technologies for rocket structures. *J. of the JWS*, 62(**8**), 46–52.

ORCID

T.M. Labur: 0000-0002-4064-2644,
A.G. Pokliatskyi: 0000-0002-4101-2206,
V.A. Koval: 0000-0001-5154-1446

CONFLICT OF INTEREST

The Authors declare no conflict of interest

CORRESPONDING AUTHOR

A.G. Pokliatskyi
E.O. Paton Electric Welding Institute of the NASU
11 Kazymyr Malevych Str., 03150, Kyiv, Ukraine.
E-mail: pag556a@gmail.com

SUGGESTED CITATION

T.M. Labur, A.G. Pokliatskyi, V.A. Koval (2024) Consumable and nonconsumable electrode welding of high-strength 2219-T31 aluminium alloy. *The Paton Welding J*., **5**, 18–27.

JOURNAL HOME PAGE

https://patonpublishinghouse.com/eng/journals/tpwj

Received: 08.02.2024
Received in revised form: 11.03.2024
Accepted: 23.05.2024